Atmos. Chem. Phys. Discuss., 12, 14623–14667, 2012
www.atmos-chem-phys-discuss.net/12/14623/2012/
doi:10.5194/acpd-12-14623-2012

Atmospheric Chemistry and Physics Discussions

Impact of natural and anthropogenic aerosols on stratocumulus and precipitation in the Southeast Pacific: a regional modelling study using WRF-Chem

Q. Yang[1], W. I. Gustafson Jr.[1], J. D. Fast[1], H. Wang[1], R. C. Easter[1], M. Wang[1], S. J. Ghan[1], L. K. Berg[1], L. R. Leung[1], and H. Morrison[2]

[1]Pacific Northwest National Laboratory, Richland, WA, USA
[2]National Center for Atmospheric Research, Boulder, CO, USA

Received: 21 May 2012 – Accepted: 24 May 2012 – Published: 8 June 2012

Correspondence to: Q. Yang (qing.yang@pnnl.gov)

Published by Copernicus Publications on behalf of the European Geosciences Union.

Abstract

Cloud-system resolving simulations with the chemistry version of the Weather Research and Forecasting (WRF-Chem) model are used to quantify the relative impacts of regional anthropogenic and oceanic emissions on changes in aerosol properties, cloud macro- and microphysics, and cloud radiative forcing over the Southeast Pacific (SEP) during the VAMOS Ocean-Cloud-Atmosphere-Land Study Regional Experiment (VOCALS-REx) (15 October–16 November 2008). Two distinct regions are identified. The near-coast polluted region is characterized by the strong suppression of non-sea-salt particle activation due to sea-salt particles, a dominant role of first over second indirect effects, low surface precipitation rates, and limited impact of aerosols associated with anthropogenic emissions on clouds. The effects of natural marine aerosols on cloud properties (e.g., cloud optical depth and cloud-top and cloud-base heights), precipitation, and the top of atmosphere and surface shortwave fluxes counteract those of anthropogenic aerosols over this region. The relatively clean remote region is characterized by large contributions of aerosols from non-local sources (lateral boundaries), much stronger drizzle at the surface, and high aerosol-cloud-precipitation interactions under a scenario of five-fold increase in anthropogenic emissions. Clouds in this clean region are quite sensitive (e.g., a 13 % increase in cloud-top height and a 9 % increase in surface albedo) to a moderate increase (25 % of the reference case) in cloud condensation nuclei (CCN) concentration produced by a five-fold increase in regional anthropogenic emissions. The reduction of precipitation due to this increase in anthropogenic aerosols more than doubles the aerosol lifetime in the clean marine boundary layer. Therefore, the aerosol impacts on precipitation are amplified by the positive feedback of precipitation on aerosol, which ultimately alters the cloud micro- and macro-physical properties, leading to strong aerosol-cloud-precipitation interactions. The high sensitivity is also related to an increase in cloud-top entrainment rate (by 16 % at night) due to the increased anthropogenic aerosols. The simulated aerosol-cloud-precipitation interactions due to the increased anthropogenic aerosols have a stronger diurnal cycle

ACPD
12, 14623–14667, 2012

over the clean region compared to the near-coast region with stronger interactions at night. During the day, solar heating results in more frequent decoupling of the cloud and sub-cloud layers, thinner clouds, reduced precipitation, and reduced sensitivity to the increase in anthropogenic emissions. The results of this study imply that the energy balance perturbations from increased anthropogenic emissions are larger in the more susceptible clean environment than in already polluted environment and is larger than possible from first indirect effect alone.

1 Introduction

Anthropogenic aerosols change the energy balance of the Earth's climate system through the direct effect of absorbing and scattering radiation as well as indirect effects of changing cloud albedo (first indirect effect) and precipitation (second indirect effect). The first indirect effect was first postulated by Twomey (1977) to describe the brightening of clouds due to smaller and more numerous cloud droplets in response to an increase in cloud condensation nuclei (CCN) at constant liquid water content. The second indirect effect describes how increases of CCN suppress rain formation, leading to longer cloud lifetime, larger liquid water path (LWP), and greater cloudiness (Albrecht, 1989). The large uncertainties related to aerosol direct and first indirect effects limit our understanding of the anthropogenic forcing on the climate system (Solomon, 2007). The second indirect effect is less well understood than the first and is even more difficult to quantify in climate models. With varying representations of aerosols, clouds, and their interactions with radiation, previous modeling studies estimated global mean top-of-atmosphere (TOA) radiative forcings range from -0.5 to $-1.9\,\mathrm{W\,m^{-2}}$ and from -0.3 to $-1.4\,\mathrm{W\,m^{-2}}$ due to the first and second indirect effects, respectively (Thomas et al., 2011 and references therein).

Over the ocean, the effect of anthropogenic aerosols is counteracted by that of large sea-salt particles. Sea-salt particles are emitted from the ocean through sea spray, bubble bursting, and spume associated with wave-breaking (Gong et al., 1997), and

ACPD
12, 14623–14667, 2012
Aerosol impact on clouds and precipitation
Q. Yang et al.

their emission strength is wind-speed dependent. Sea-salt particles are hygroscopic and have larger surface areas than anthropogenic aerosols, such as sulfate. Therefore, the condensation of gaseous sulphuric acid and water preferentially occur on them, thus inhibiting new particle formation, lowering the maximum supersaturation in clouds and suppressing the activation of anthropogenic aerosols in clouds (Ghan et al., 1998). Sea-salt particles could also serve as giant (e.g., > 2 µm) and ultra-giant (e.g., > 10 µm) CCN, and they have been found to decrease total droplet number, promote drizzle production, and reduce LWP in polluted clouds (e.g., Feingold et al., 1999; Lu and Seinfeld, 2005; Rosenfeld et al., 2002).

The oxidation of dimethyl sulfide (DMS) is a source of secondary aerosols, non-sea-salt sulfate aerosol over the ocean. Charlson et al. (1987) postulated that an increase in DMS emissions could exert a cooling effect on the climate system (Charlson et al., 1987). However, using simulations from several climate models Woodhouse et al. (2010) found a relatively weak climate response to DMS due to the low sensitivity of CCN concentrations to the change in DMS emissions.

Marine stratocumulus clouds are ideal for studying the relative roles of natural and anthropogenic aerosols in changing cloud properties and radiative forcings. This is because their overall cooling effect is important to the earth's energy budget and also because these boundary layer clouds are often close to emission sources. With a large and persistent stratocumulus cloud deck (Klein and Hartmann, 1993) and a complex mixture of aerosols from anthropogenic and marine sources (Chand et al., 2010; Kleinman et al., 2012; Shank et al., 2012), the Southeast Pacific (SEP) is an ideal location for studying effects of aerosols on shallow warm clouds. Observations from the VAMOS Ocean-Cloud-Atmosphere-Land Study Regional Experiment (VOCALS-REx; Wood et al., 2011b) show distinctly different cloud and precipitation features over the remote and near-coast regions over the SEP associated with low and high concentrations of CCN (e.g., Bretherton et al., 2010; Painemal and Zuidema, 2010; Wood et al., 2011a; Zheng et al., 2011; Zuidema et al., 2012), which resemble the pristine

ACPD
12, 14623–14667, 2012

precipitating and the polluted non-precipitating cloud regimes predicted by previous studies (e.g., Baker and Charlson, 1990).

Process models, such as large-eddy simulations (LES) and Mixed Layer Models (MLM), have often been used to study marine stratocumulus clouds. MLM are used to study the steady state solutions of a group of thermodynamic equations with fixed external forcings such as mean subsidence, sea surface temperature (SST), and lower-tropospheric divergence (e.g., Bretherton and Wyant, 1997; Pincus and Baker, 1994; Stevens, 2006; Wood, 2007). The main advantage of the LES is its ability to resolve turbulent eddies and cloud microphysical processes within them. LES are often idealized and conducted in small domains (on the order of 10^2 km^2 or smaller) to study the equilibrium state or diurnal cycle of clouds under horizontally uniform forcing conditions (e.g., Berner et al., 2011; Chen et al., 2011; Lu and Seinfeld, 2005; Sandu et al., 2008; Wang and McFarquhar, 2008a, b). With a relatively large domain (on the order of 10^4 km^2), the LES can simulate the response of mesoscale cloud structures to aerosol perturbations, but only in very ideal meteorological scenarios with prescribed large-scale forcings (Kazil et al., 2011; Mechem et al., 2012; Wang and Feingold, 2009a, b).

The climate modeling community is actively engaged in improving the presentation of aerosol and aerosol-cloud-radiation interactions in regional and global models. Increased computational resources have permitted the application of regional models with prognostic aerosols and coupled aerosol-cloud-radiation processes, such as the chemistry version of the Weather Research and Forecast model (WRF-Chem, Fast et al., 2006; Grell et al., 2005), to the study of aerosol-cloud interactions (ACI) under realistic meteorological conditions. The use of realistic meteorological conditions allows for simulating complex interactions between clouds and meteorological factors and their feedbacks to larger-scale dynamics. In addition to LES and MLM, regional models with interactive aerosols and coupled aerosol-cloud-radiation processes can be important tools for advancing our understanding of aerosol effects on regional climate.

ACPD
12, 14623–14667, 2012

WRF-Chem has been used in a wide range of applications including air quality, aerosol-cloud-precipitation studies, and regional climate (e.g., Fast et al., 2012; Gao et al., 2011; Qian et al., 2009; Zhang et al., 2010). Yang et al. (2011) and Saide et al. (2012) evaluated WRF-Chem simulations of aerosols, clouds, precipitation, and their interactions over the SEP during VOCALS-REx using extensive measurements from the field campaign and satellite retrievals. Comparisons with observations showed that the model performed well in simulating aerosol (e.g., AOD, accumulation mode aerosol number, submicron aerosol mass) and clouds (e.g., cloud top and cloud base height, cloud fraction cloud water path). The well-simulated cloud properties fed back to the dynamics and improved the simulated boundary-layer characteristics as well as surface and top-of-atmosphere (TOA) energy fluxes. Q. Yang et al. (2011) and Saide et al. (2012) also demonstrated that WRF-Chem was able to simulate the synoptic-scale variations of aerosol and cloud properties over the SEP in response to the pollution outflow from South America.

In this study, WRF-Chem simulations are used to quantify and compare the impacts of anthropogenic and natural oceanic emissions on aerosol properties, cloud macro- and microphysics, and cloud radiative forcings over the SEP during VOCALS-REx. Aerosol-cloud-precipitation interactions in polluted and clean regions are investigated. To our knowledge, this is the first use of a regional model with prognostic aerosols and coupled aerosol-cloud-radiation to study the relative contributions of oceanic and anthropogenic aerosols to changes in cloud properties and radiative forcings over the SEP under realistic meteorological conditions at cloud-system resolving scale. The analysis is based on month-long simulations. Thus, the results represent responses to varying synoptic conditions over a longer time period than those in typical LES and MLM modeling studies, and hence can provide insights into the aerosol-cloud-precipitation interactions and their impact on climate.

The remainder of this paper is organized as follows. The WRF-Chem model and the simulations are described in Sect. 2. The response of aerosol number concentrations and optical properties to regional anthropogenic and oceanic emissions is discussed

Discussion Paper | Discussion Paper | Discussion Paper | Discussion Paper |

ACPD

12, 14623–14667, 2012

Aerosol impact on clouds and precipitation

Q. Yang et al.

in Sect. 3.1. The response of cloud microphysical and optical properties is presented in Sect 3.2, followed by cloud macro-properties, precipitation, and radiative forcing in Sects. 3.3, 3.4, and 3.5, respectively. Finally, Sect. 4 summarizes the main conclusions and implications of this study.

2 Model description and experimental design

The WRF-Chem model includes full online interactions between aerosols, radiation, clouds and precipitation for the direct, semi-direct, and first and second indirect effects of aerosols as described in Fast et al. (2006), Chapman et al. (2009), Gustafson et al. (2007), and Q. Yang et al. (2011). The simulations presented in this study were performed using the code that was released to the public in v3.3. The detailed model description and configuration can be found in Q. Yang et al. (2011), and here the model configuration is only briefly summarized.

The MOdel for Simulating Aerosol Interactions and Chemistry (MOSAIC, Zaveri et al., 2008) is used with an 8-bin sectional approach to represent aerosol size distributions. The cloud microphysics is represented with the Morrison double-moment scheme (Morrison et al., 2009) that was recently coupled with interactive aerosols (Q. Yang et al., 2011). The YSU scheme (Hong et al., 2006) is used to represent vertical mixing associated with the boundary layer. In the YSU scheme, the non-local mixing due to large eddy transport is considered for heat and momentum components, and an explicit treatment of entrainment is included in the heat and moment flux profiles and the growth of the planetary boundary layer (PBL) height (Noh et al., 2003; Shin and Hong, 2011). Excluding five days of model spin-up, simulations are conducted from 00:00 UTC 15 October to 00:00 UTC 16 November in 2008. The model domain is roughly from 63° W to 93° W in longitude and from 11° S to 36° S in latitude and includes parts of the Northern Chilean and Southern Peruvian coasts and the nearby Southeast Pacific (see Fig. 1). The horizontal grid spacing is 9-km and the vertical grid spacing increases from ~ 30 m near the ocean surface to ~ 50 m at 1 km height. Initial

ACPD
12, 14623–14667, 2012

and boundary conditions for meteorology and time dependent sea surface temperatures were obtained from the Global Forecast System (GFS) with a 0.5-degree grid spacing, while the initial and boundary conditions for trace gases and aerosols were provided by the global Model for OZone and Related chemical Tracers (MOZART).

The simulation described and evaluated by Q. Yang et al. (2011; called the AERO experiment therein) is used as our reference simulation (REF hereafter). The emission inventory compiled for the VOCALS model assessment provides anthropogenic emissions including both point and area sources. Ultrafine, fine, and coarse mode ($< 10\,\mu$m) sea-salt emissions are parameterized based on Clarke et al. (2006), Gong et al. (1997), and Monahan et al. (1986), respectively. DMS emissions are based on a simplified Nightingale et al. (2000) scheme. A detailed description of the emissions and the coupling of aerosol-cloud-radiation processes can be found in Q. Yang et al. (2011).

One challenge in studying cloud-aerosol interactions is the difficulty in separating the aerosol-induced changes from meteorology-induced changes in cloud properties because aerosol and meteorological characteristics tend to be correlated (Loeb and Schuster, 2008; Stevens and Feingold, 2009). Therefore, for the purpose of quantifying separately the effects of different emission sources within the model domain, three sensitivity runs (Table 1) are conducted with one simulation having anthropogenic emissions turned off (0ANT), one with primary (sea salt) and secondary precursor (DMS) oceanic emissions turned off (0OCE), and one with anthropogenic emissions increased by a factor of 5 (5ANT). We acknowledge that a factor of 5 is arbitrary; however, the purpose is to produce a significant increase in anthropogenic aerosols over the remote ocean ($\sim 13\,\text{cm}^{-3}$ increase in CCN). The results are, therefore, an extreme condition, and the magnitude of the influence would likely be smaller for changing anthropogenic emissions under most scenarios, although we expect that the tendency of the results will likely be the same.

The effects of regional anthropogenic and oceanic emissions are estimated by contrasting sensitivity simulations with the reference simulation, REF. The effect of anthropogenic emissions from continental sources within the domain (AnthroEmis) is

Discussion Paper | Discussion Paper | Discussion Paper | Discussion Paper |
ACPD
12, 14623–14667, 2012
Aerosol impact on clouds and precipitation
Q. Yang et al.

calculated as the difference in simulated quantities between REF and 0ANT. Similarly, the regional oceanic emission (OceanEmis) effect is calculated as the difference between REF and 0OCE. The effect of the increased anthropogenic emissions (ScaledEmis) is defined as the difference between 5ANT and REF. Contrasting sensitivity simulations with REF facilitates the estimation of emission-induced changes, and isolates the impacts due to the differences in meteorology.

To assist with the diagnosis, additional 10-day sensitivity simulations (excluding spin-up periods) are also conducted. The first supplementary sensitivity simulation turns off boundary conditions of gas and aerosol species, the second has no DMS emission but retains sea-salt emissions, and the third turns off the new particle nucleation process.

The aerosol direct radiative forcing at the surface is calculated as the difference in surface shortwave fluxes under cloud-free conditions with and without aerosols. The current version of WRF-Chem does not compute the aerosol direct forcing on-line, so an off-line utility (Barnard et al., 2010) that mimics the radiation routine in WRF-Chem was used to calculate the direct aerosol and cloud forcing for the REF simulation.

3 Aerosol, cloud, precipitation, and energy flux responses to regional emissions

The aerosol index (AI) is dominated by contributions from anthropogenic aerosols (compared to sea-salt and dust; Matsui et al., 2006), and is used to illustrate the strong anthropogenic influence over the SEP. The AI is calculated as the product of AOD at 550 µm and the Ångström coefficient between 400 µm and 700 µm. Q. Yang et al. (2011) showed that the simulated AOD at 550 µm agrees well with the MODIS retrievals in mean spatial distribution pattern and the domain average (0.10 ± 0.06 and 0.11 ± 0.06 for the MODIS and REF, respectively) during VOCALS-REx. The horizontal distribution of the monthly-average AI over the ocean is shown in Fig. 1 for the REF simulation. The large gradient in AI near the coast reflects the strong influence from continental emission sources. This is consistent with the observed longitudinal gradient of aerosol

ACPD
12, 14623–14667, 2012

Aerosol impact on clouds and precipitation

Q. Yang et al.

concentrations during VOCALS-REx (e.g., Allen et al., 2011; Bretherton et al., 2010; Hawkins et al., 2010). For the purpose of contrasting emission effects at different regions over the ocean, the marine area within the domain (excluding areas close to lateral boundaries) is divided into 9 regions (numbered by 1–9, Fig. 1) with the regions 3–8 being $5^{\circ} \times 5^{\circ}$ in size. Three specific regions 3, 4, and 7 with high, intermediate, and low AI values, which represent polluted (region P), intermediate (region I), and clean (region C) marine environments, respectively, have been selected for detailed analysis. These three regions are also differentiated by their relative distances from the coastline. The selection intentionally avoids regions close to the southern inflow boundary. The selected regions also correspond to low (region P), intermediate (region I) and high (region C) values of the aerosol-cloud interaction indices, which will be discussed later in this section.

3.1 Aerosol

Figure 2a, b shows the contributions of regional oceanic (OceanEmis), anthropogenic (AnthroEmis), and enhanced anthropogenic emissions (ScaledEmis) to number concentrations of accumulation mode aerosols (N_{acc}) and CCN (N_{CCN}, at supersaturation $s = 0.1\,\%$) at ~ 975 hPa. The selection of N_{CCN} at $s = 0.1\,\%$ follows previous VOCALS studies (Bretherton et al., 2010; Q. Yang et al., 2011). In this study, we use accumulation mode aerosols to refer to particles with dry diameters of 0.078–1.25 µm with most of those particles in the 0.078–0.31 µm dry diameter range. The average contribution of the regional oceanic emissions to N_{acc} increases from 2 % ($\Delta N_{acc} = 10\,cm^{-3}$) over region P to 10 % ($\Delta N_{acc} = 27\,cm^{-3}$) over region C. OceanEmis contributions to N_{CCN} are larger: 20 % ($\Delta N_{CCN} = 27\,cm^{-3}$), 39 % ($\Delta N_{CCN} = 33\,cm^{-3}$), and 46 % ($\Delta N_{CCN} = 25\,cm^{-3}$) for regions P, I, and C, respectively.

Regional anthropogenic emissions contribute 33 % ($\Delta N_{acc} = 129\,cm^{-3}$ and $\Delta N_{CCN} = 46\,cm^{-3}$) to N_{acc} and N_{CCN} over region P, and their contribution decreases to ~ 10 % ($\Delta N_{acc} = 25\,cm^{-3}$ and $\Delta N_{CCN} = 9\,cm^{-3}$) over region I and ~ 0 % over the more remote

ACPD
12, 14623–14667, 2012

region C. Consistent with the climatology over the SEP, a persistent surface-high pressure system was centered near 95° W, 32° S during VOCALS-REx, and the marine boundary layer (MBL) air circulates around the center of the high pressure system. The streamlines in Fig.13a of Toniazzo et al. (2011) showed predominant marine influence over region C by horizontal transport.

The high $\frac{\Delta N_{\mathrm{CCN}}}{\Delta N_{\mathrm{acc}}}$ ratios for OceanEmis (0.92–2.7 over the three regions) compared to AnthroEmis (0.36 over both regions P and I) are due to a combination of the larger hygroscopicity and the larger sizes of sea-salt particles. The simulated aerosol size distributions (figures not shown) also suggest that the addition of sea-salt particles inhibit the growth of small non-sea-salt particles (dry diameter < 0.078 µm) to accumulation mode size. This simulated inhibition is only present over the polluted region P, and it contributes to the low ΔN_{acc} from OceanEmis over this region (Fig. 2a). A supplementary simulation with DMS emissions turned off indicates that DMS emissions lead to a 6 % increase in N_{acc} over region P, but its contribution to N_{acc} is reduced away from the coast with a negligible contribution over region C. Associated with the overprediction of the DMS emission scheme under high-wind conditions (Blomquist et al., 2006), the simulated DMS ocean-to-air transfer velocity was overestimated by about 70 % compared to observations (Q. Yang et al., 2011); thus the actual DMS effect might be even smaller.

When subtracting N_{acc} and N_{CCN} contributed by both AnthroEmis and OceanEmis from their mean total concentrations in the REF, the residuals account for aerosols originating from lateral boundaries, natural aerosols originating from continental sources, and the likely non-linear responses of N_{acc} and N_{CCN} to changes in emissions. A supplementary sensitivity simulation (BND, not shown) with no aerosols and gas chemical species from the lateral boundaries shows 85 % (region I) and 95 % (region C) reductions of both N_{acc} and N_{CCN} concentrations from those of the REF, suggesting a dominant aerosol influence from outside the model domain for regions I and C. Over region P, contrasting the BND and REF simulations indicates that ~ 35 % of N_{acc} and N_{CCN} originate from lateral boundaries. The southern boundary of the model domain

ACPD
12, 14623–14667, 2012

is the main low-level inflow boundary during VOCALS-REx. Southeasterly winds prevail within the MBL with reduced wind speed towards the coast during VOCALS-REx (Rahn and Garreaud, 2010), and mean surface winds are approximately southerly at 20° S near the coast, and southeasterly (125°) at 20° S, 85° W (Toniazzo et al., 2010).

With the five-fold increase in anthropogenic emissions, the $\Delta N_{CCN}/\Delta N_{acc}$ has higher values of 0.54 and 0.51 over more polluted regions P and I, respectively, and a lower value of 0.28 over relatively clean region C. The mean N_{CCN} increased by 90 % (120 cm^{-3}), 44 % (37 cm^{-3}), and 25 % (13 cm^{-3}) over regions P, I, and C, respectively.

The relationships between emission strength and N_{acc} are nonlinear for both oceanic and anthropogenic emissions. For example, the response of N_{acc} to ScaledEmis in each region is not four-times the response to AnthroEmis. This is associated with the highly nonlinear nature of aerosol processes including nucleation, coagulation, condensational growth of existing particles from gas-phase chemicals (such as the uptake of gas-phase H_2SO_4 by sea-salt particles), and wet removal.

The AOD response to different emissions is shown in Fig. 2d. Regional oceanic emissions have large contributions (40–50 %; 0.05–0.06) to AOD over all three regions, mostly due to sea-salt particles. Mean 10-m wind speeds and sea-salt emissions over regions C and I are about twice as large as region P; however, the wet removal is also stronger over regions C and I. Over region P, AnthroEmis contributes only about half as much to AOD compared to that of OceanEmis, and its contributions are negligible over regions I and C.

3.2 Cloud microphysical and optical properties

The changes in cloud properties due to emissions are discussed below in terms of absolute and relative changes as well as ACI indices in order to contrast ACI strength in the three regions. Following studies in the current literature (e.g., Feingold et al., 2001; Quaas et al., 2009; Wang et al., 2011), we define ACI as the relative change in a mean cloud property (e.g., LWP and r_e) between sensitivity simulations and the REF with respect to the change in some measure of the aerosol in a column (i.e.,

Discussion Paper | Discussion Paper | Discussion Paper | Discussion Paper |
ACPD
12, 14623–14667, 2012

a proxy, such as AI). For the purpose of evaluating ACI of boundary layer clouds due to either oceanic or anthropogenic emissions, CCN at ~ 975 hPa is chosen as the proxy. Therefore, when evaluating the cloud property responses to emissions, the ACI indices are defined as $\mathrm{ACI_{CNN}}(Y) = \frac{\Delta \ln(Y)}{\Delta \ln(\mathrm{CCN})}$, where Y is a cloud property. Those ACI index values are shown in red in Fig. 2c, e, and f and Fig. 3.

The cloud-top droplet number concentration (N_d) increases with increasing anthropogenic emissions (Fig. 2c). Regional anthropogenic emissions (AnthroEmis) contribute 34 % (46 $\mathrm{cm^{-3}}$) and 8 % (9 $\mathrm{cm^{-3}}$) to N_d over regions P and I, respectively. The $\mathrm{ACI_{CCN}}$ (N_d) values are 0.83, 0.82, and 1.36 over regions P, I, and C with ScaledEmis, and the higher index over region C indicates more efficient aerosol activation over the clean marine environment. Increased anthropogenic emissions (ScaledEmis) lead to a 36 % (26 $\mathrm{cm^{-3}}$) increase in the mean N_d concentration over region C.

The addition of oceanic emissions, in contrast, decreases N_d by 27 % (37 $\mathrm{cm^{-3}}$), 12 % (13 $\mathrm{cm^{-3}}$), and 5 % (3 $\mathrm{cm^{-3}}$) over regions P, I, and C, respectively. Ghan et al. (1998) found that the competition for water vapor between large sea-salt particles and submicron particles (e.g., non-sea-salt sulfate) lowers the maximum supersaturation in a cloud updraft, and thus suppresses the activation of the more numerous submicron particles. As was described in Sect. 3.1 with respect to ΔN_acc, sea-salt particles inhibit some fine non-sea-salt particles from growing to viable CCN sizes, and this could also contribute to the reduction in N_d. The sea-salt suppression of droplet activation from non-sea-salt particles is most pronounced over the polluted region as shown by the more negative $\mathrm{ACI_{CCN}}(N_\mathrm{d})$ of −1.1 over region P compared to that of region C (−0.1), consistent with Ghan et al. (1998). The decrease in N_d due to the sea-salt suppression effect dominates the increase in N_d due to secondary oceanic emissions (DMS oxidation; ΔN_d =~ 8 %).

The cloud-top droplet effective radius, r_e, is calculated directly within the microphysics scheme based on the predicted droplet size distributions. As shown in Fig. 2e, anthropogenic aerosols (AnthroEmis and ScaledEmis) reduce r_e over region P, reflecting the first indirect effect. Over this region, anthropogenic aerosols induce a 12 %

ACPD
12, 14623–14667, 2012

(1.2 µm) decrease in r_e, and half of this effect is cancelled by the opposite effect of sea-salt. This is consistent with the mitigation of anthropogenic aerosol indirect effect by sea-salt aerosols proposed by Rosenfeld et al. (2002). In region C, the addition of $\sim 13\,\text{cm}^{-3}$ CCN (25 % increase) leads to a 35 % (−4.2 µm) reduction of mean r_e. By definition, the first indirect effect assumes constant liquid water content, and Feingold et al. (2003) proposed a theoretical upper limit of 0.33 for indirect effect (similar to $-\text{ACI}_{\text{CCN}}$ (r_e)) for a homogenous cloud with constant liquid water content. The simulated ACI indices over the region P are within this limit. However, the large changes in r_e due to the relatively small increase in anthropogenic aerosols over region C indicate dynamic feedbacks and aerosol second indirect effect, which are discussed in more detail in Sect. 3.4. Associated with the increased sensitivity of clouds to anthropogenic aerosols over region C, the east-west gradient of the response to AnthroEmis is reversed with ScaledEmis with the largest response over region C.

The changes in cloud optical depth (COD) are consistent with the large changes in r_e. Anthropogenic emissions contribute a 4–14 % increase in COD, which is counteracted by the 7–9 % reduction induced by the sea-salt particles. Related to the stronger sea-salt effect in suppressing small particle activation over the polluted region, region P has the largest reduction (−1.8; 10 %) in COD due to OceanEmis, followed by regions I (−1.5; 8 %) and C (−0.5; 4 %). In the clean region C, COD is more sensitive to ScaledEmis ($\text{ACI}_{\text{CCN}} = 1.9$) compared to region P (0.3–0.4). A relatively small increase in N_d ($26\,\text{cm}^{-3}$; 36 %) in region C due to ScaledEmis leads to a 54 % increase in COD, which has a major contribution from changes in LWP (discussed in Sect. 3.3).

3.3 Cloud macro-properties

This section discusses the changes in cloud heights, cloud thickness, cloud fraction, and liquid water path with emissions. These simulated cloud properties in REF have been evaluated against observations in Q. Yang et al. (2011), and an overall good agreement in the features of the distribution and mean values were demonstrated. For example, the simulated mean cloud-top height (approximation of MBL heights) and

ACPD
12, 14623–14667, 2012

mean cloud thickness in REF agree with observations within 10 %, and the simulated cloud fraction has a mean low bias of 2–3 % during VOCALS-REx (Q. Yang et al., 2011).

As shown in Fig. 3a, sea-salt emissions reduce the mean cloud-top heights by 13–18 m over the three regions, while regional anthropogenic emissions elevate the mean cloud-top heights by 14 and 10 m over regions P and I, respectively. These changes are small but statistically significant, and the 98 % confidence intervals for the mean changes are shown as error bars in Fig. 3. With the increased anthropogenic emissions, stronger responses are seen in the cloud-top (Z_t) and cloud-base heights (e.g., $\mathrm{ACI_{CCN}}(Z_t = 0.56$; and $\Delta Z_t = 174$ m, which is 13 % of REF) over region C compared to those over region P (e.g., $\mathrm{ACI_{CCN}}(Z_t = 0.10$; $\Delta Z_t = 65$ m, which is 6 % of REF).

The changes in cloud-top heights due to anthropogenic and oceanic aerosols are also linked to cloud-top entrainment. Entrainment is an important process related to water and static energy distributions within the MBL, and transport of aerosols from the free troposphere (e.g., Raes, 1995; M. Yang et al., 2011). Based on LES simulations of marine stratocumulus clouds, Ackerman et al. (2004) found that cloud-top entrainment increases with increasing N_d. A later study by Bretherton et al. (2007) linked the N_d-induced entrainment change with droplet sedimentation. Studying a nocturnal non-drizzling stratocumulus layer using LES with bulk microphysics, cloud droplet sedimentation was found to decrease entrainment rates because removal of liquid water from the entrainment zone reduces both evaporative cooling and longwave radiative cooling, with evaporative cooling found to be more important than radiative cooling in changing entrainment rates (Bretherton et al., 2007). In our simulations, cloud droplet sedimentation in the double-moment Morrison microphysics scheme depends explicitly on droplet size distribution. An increase in N_d leads to smaller droplet sizes resulting in reduced droplet sedimentation velocity. Therefore, an increase in anthropogenic aerosols leads to smaller cloud droplets, which reduce cloud droplet sedimentation, and results in an increase in entrainment rate (Bretherton et al., 2007; Hill et al., 2009) and higher cloud tops. Additional 4-day sensitivity simulations with droplet size fixed

ACPD
12, 14623–14667, 2012

Title Page
Abstract | Introduction
Conclusions | References
Tables | Figures
◀| |▶
◀ ▶
Back | Close
Full Screen / Esc
Printer-friendly Version
Interactive Discussion

for calculation of sedimentation in REF and 5ANT (assuming an effective radius of 12 µm), thereby excluding interactions between N_d, sedimentation, and entrainment, support the interpretation that impact of N_d on sedimentation account for most of the changes in cloud-top entrainment. The increase in cloud-top entrainment rates is more pronounced with ScaledEmis.

Cloud-top entrainment rates in the simulations are estimated using a budget analysis (Eq. 4 of Yang et al., 2009) of an artificial passive tracer, as described in Q. Yang et al. (2011). Note that this entrainment is different from the parameterized PBL entrainment in the YSU scheme (S. Hong, personal communication, 2012). The nighttime entrainment rates over regions P, I and C increase by 3 %, 6 % and 16 % in 5ANT compared to the REF. Due to the increased entrainment, the changes in temperature (virtual potential temperature, θ_v), and humidity (water vapor mixing ratio, q_v) within the inversion layer are larger over region C compared to P (1.3 vs. 0.78 g kg^{-1} in Δq_v and −1.84 vs. −1.27 K in $\Delta\theta_v$). More entrained dry air due to the increased entrainment is likely to contribute, at least in part to the less humid ($\Delta q_v = -0.2$ g kg^{-1}) MBL simulated in 5ANT compared to the REF. Note that the simulated drier and warmer ($\Delta T = 0.2$ K) MBL is consistent with higher cloud-base heights (Fig. 3b).

Larger sensitivity of cloud-top heights to N_d changes are found over regions C. Oceanic emissions contribute very little to the mean N_d over regions C compared to P (see Fig. 2c, −5 %/−3 cm^{-3} vs. −27 %/ − 37 cm^{-3}), and yet they result in a similar mean response to cloud-top heights. The larger sensitivity of MBL heights to N_d changes over region C is likely related to the more important role of sedimentation over the clean region. It is also likely that the simulated drier and colder air overlying the MBL ($q_v = 0.91$ and 2.3 g kg^{-1}, and $\theta_v = 303.8$ and 308.2 K over regions C and P, respectively, at 2 km height), when entrained into MBL, has a larger effect of enhancing droplet evaporation. These differences in sensitivity may also be driven by changes in the response of mesoscale dynamics between C and P. In addition, over the clean region, reduced precipitation (∼ 65 % reduction in cloud-base and near-surface rain rate) due to anthropogenic aerosols leads to a reduction of both below-cloud evaporative

ACPD
12, 14623–14667, 2012

cooling and in-cloud latent heat release, resulting in stronger turbulence and thus an increase in the kinetic energy available for the cloud-top entrainment (Lu and Seinfeld, 2005; Wood, 2007). Q. Yang et al. (2011) showed good agreement between the model-predicted and observed temperature and humidity profiles over the remote region (78–88° W, along 20° S) during VOCALS-REx. However, over the coastal region (east of 78° W, along 20° S), comparisons with dropsonde (Bretherton et al., 2010) and radiosonde (de Szoeke et al., 2010) measurements found larger mean humidity biases of ~ 1.6–$2.2\,\mathrm{g\,kg^{-1}}$ in the layer above MBL and below 2 km. It is likely that over region P, the simulated humidity in the layer right above the MBL is biased high, which is likely to reduce some of the predicted cloud height sensitivity to N_d, although for the polluted conditions over region P the near cloud-top droplet sedimentation flux over region P is much smaller compared to region C.

The cloud-base height response is similar to that of cloud-top height for both regional anthropogenic and oceanic emissions (Fig. 3b). Cloud depth (D_{cld}) thus has minor changes due to regional oceanic ($\Delta D_{cld} = -1$ to -2 m over the three regions) and anthropogenic emissions ($\Delta D_{cld} = 3$ and ~ 0 m over region I and P, respectively). The response of D_{cld} to ScaledEmis is also negligible in the polluted region P. The changes in liquid water path (LWP) are consistent with the changes in cloud depth. The insensitivity of D_{cld} and LWP to both anthropogenic and oceanic emissions over region P indicates that the change in surface precipitation due to emissions is insufficient to modify D_{cld} and LWP over this region. The limited impact of aerosols on D_{cld} and LWP is also consistent with their limited impact on entrainment over region P as discussed above.

The cloud thickness and LWP are more sensitive to the increased anthropogenic emissions over the clean remote region than over the polluted region. Clouds were able to develop into a deeper state ($\Delta D_{cld} = 11\,\%$ and 40 m; $\Delta \mathrm{LWP} = 41\,\%$ and $41\,\mathrm{g\,m^{-2}}$) over the clean marine region with the addition of anthropogenic aerosols. This is consistent with results from Pincus and Baker (1994) who predicted that cloud thickness increases with N_d, especially at low N_d conditions using a simple diurnally averaged

ACPD
12, 14623–14667, 2012

steady-state mixed layer model. When anthropogenic aerosols are added over the clean region C, the increase in D_{cld} and LWP due to lower precipitation (a weaker cloud water sink) dominate the reduction due to more entrainment of dry air. This results in a net increase in D_{cld}, LWP, and low cloud fraction (f_{low} is defined as cloud frequency below 700 hPa; Fig. 3e). $\mathrm{ACI_{CCN}}$(LWP) is as large as 1.5, which is associated with large responses in cloud thickness ($\mathrm{ACI_{CCN}}(D) = 0.5$), cloud frequency ($\mathrm{ACI_{CCN}}(f_{\mathrm{low}}) = 0.4$), and cloud water mixing ratios ($\mathrm{ACI_{CCN}}(q_c) = 1.1$).

Diurnal cycles of Z_t, Z_b, LWP, D_{cld}, and f_{low} (not shown) reveal that their responses to anthropogenic emissions over region C are most pronounced at night, and are very small between 14:00 and 20:00 local standard time (LST). The sensitivity of cloud macro-physical properties to N_d variations is reduced during the daytime because the absorption of solar radiation in the cloud layer offsets the cloud-top longwave radiative cooling and reduces convective mixing (Ackerman et al., 2003, 2004; Lu and Seinfeld, 2005). Solar heating was found to lead to more frequent decoupling of the cloud layer from the sub-cloud layer (e.g., Nicholls, 1984). Following Jones et al. (2011), decoupling is diagnosed from simulation results using humidity and potential temperature. Based on differences between the MBL layer below the inversion and the near-surface layer, the presence of moisture ($\Delta q_v > 0.5\,\mathrm{g\,kg^{-1}}$) and/or temperature jumps ($\Delta\theta_v > 0.5\,\mathrm{K}$) indicates a decoupling event. In cloudy conditions, daytime decoupling is more frequent over region C (with daytime maximum frequency of ~ 50 % between 12:00–13:00 LST) compared to that of region P (~ 30 %) in REF. The increased daytime decoupling is also accompanied by less precipitation (diurnal minimum and maximum of 0.08 and 1.04 $\mathrm{mm\,day^{-1}}$, respectively) and thinner clouds (diurnal minimum and maximum LWP of 42 and 137 $\mathrm{g\,m^{-2}}$, respectively) over region C. Anthropogenic emissions increase daytime maximum decoupling frequencies to 33 % and 61 % over regions P and C. Sandu et al. (2008) attributed the increased daytime decoupling frequencies due to anthropogenic aerosols in polluted clouds with reduced sensible heat flux, increased entrainment, and reduced evaporation resulting from precipitation suppression; this is consistent with our results. The stronger and more frequent decoupling

Discussion Paper | Discussion Paper | Discussion Paper | Discussion Paper |
ACPD
12, 14623–14667, 2012
Aerosol impact on clouds and precipitation
Q. Yang et al.

during the daytime reduces the moisture supply to the cloud layer, and it also likely inhibits the transport of aerosols from the sub-cloud layer into the cloud layer contributing to the reduced sensitivity to emission changes compared to nighttime. This is supported by the simulated minimum N_d (~ 35 % lower than the diurnal mean) between 12:00 and 15:00 LST over region C with the enhanced anthropogenic emissions.

For a few scenarios of stratocumulus clouds over both the Northeastern Atlantic and the coast of southern California, Ackerman et al. (2004) simulated ACI_{CCN}(LWP) in the magnitude range of 0.06–0.35 using LES models. LES study by Lu and Seinfeld (2005) showed ACI_{CCN}(LWP) of 0.22 and 0.59 over polluted and clean conditions for the simulated nighttime stratocumulus cloud. Wang et al. (2011) obtained ACI_{CCN}(LWP) values (for present day versus pre-industrial aerosols) of about 0.30 and 0.10 using a traditional global climate model (CAM5) and a multi-scale aerosol-climate model, respectively. The ACI_{CCN}(LWP) values for regional anthropogenic emissions for regions P and I in this study are 0.06 and 0.18, respectively, which are comparable to those in the literature. However, with the 5-fold increase in anthropogenic emissions, the estimated ACI_{CCN}(LWP) is much higher over region C.

Over region P, OceanEmis and AnthroEmis lead to a negligible increase in low-cloud fraction (f_{low}) (< 1 %). ScaledEmis reduces f_{low}($\Delta f_{low} = -1.9$ %, on average) over region P, which is opposite to the responses over regions I and C. Further investigation reveals that the opposite response occurs over locations (upper right corner of region P; also see Fig. 8 of Q. Yang et al., 2011) that are associated with synoptic induced subsidence and are typically cloud-free or have thin clouds (LWP < $50\,\mathrm{g\,m^{-2}}$). The sedimentation effect could explain the simulated response over this near-coast area where increased N_d reduces sedimentation thus increasing entrainment rates, which contributes to the diminishing or further thinning of those thin clouds.

3.4 Precipitation responses to aerosols

Precipitation responses to aerosols over different regions are examined using probability of precipitation (POP) (e.g., L'ecuyer et al., 2009), and precipitation susceptibility

ACPD
12, 14623–14667, 2012
Aerosol impact on clouds and precipitation
Q. Yang et al.

(e.g., Sorooshian et al., 2009). These tools have been used in recent studies to examine aerosol-cloud-precipitation interactions (e.g., POP in Freud and Rosenfeld, 2012; precipitation susceptibility in Terai et al., 2011). Hourly outputs from each model grid column are used for the calculation of POP and precipitation susceptibility. POP is defined as the precipitation frequency of clouds at a given macrophysical condition, such as a fixed LWP. A precipitating event is defined as surface rain rates (R) exceeding 0.12 mm day^{-1} (i.e., 0.005 mm h^{-1}). Although POP values vary with the selection of the threshold surface rain rate, it does not alter the main conclusions drawn. A modified rain susceptibility is defined similar to ACI indices, but with an opposite sign:

$$S_{\text{ccn}} = -\frac{\Delta \ln R}{\Delta \ln N_{\text{CCN}}} = -\text{ACI}_{\text{CCN}}(R).$$

The POP as a function of LWP is shown in the first column of Fig. 4a. The POP increases with LWP and a more rapid increase is seen over region C. In REF, POP is $< 20\,\%$ for typical LWP values ($< 300\,\text{g}\,\text{m}^{-2}$, occurring at 96 % frequency) over region P, while POP values are distinctly larger ($\sim 10\,\%$ and 20 % larger during day and night, respectively) over regions C than P for typical LWP values.

Oceanic emissions facilitate rain formation as indicated by the higher POP in REF than in 0OCE. When evaluated using POP, this effect is more pronounced over the polluted region ($\text{POP}_{\text{ref}} - \text{POP}_{\text{0OCE}} = -1\,\%$ to $-7\,\%$ for LWP of 100–300 $\text{g}\,\text{m}^{-2}$) than over the clean region ($\text{POP}_{\text{ref}} - \text{POP}_{\text{0OCE}} = -1\,\%$ to $-3\,\%$ for LWP of 100–300 $\text{g}\ \text{m}^{-2}$). When evaluated using rain susceptibility, oceanic emissions also have a larger effect of facilitating rain formation over the polluted region P (–0.6) than over region C (~ 0.0). The stronger effect of oceanic emissions on the surface precipitation frequency and precipitation rate over region P is consistent with the stronger N_{d} suppression effect by sea-salt particles over region P discussed earlier.

Anthropogenic emissions suppress rain formation and reduce POP in both regions P and C. Over region P, regional anthropogenic emissions reduce POP by 2–12 % (for LWP of 100–300 $\text{g}\,\text{m}^{-2}$) in REF compared to that of 0ANT, and increased anthropogenic emissions reduce POP by 2–15 % from that of REF. The increased anthropogenic emissions have a much larger rain suppression effect over region C, where reductions in POP for 5ANT relative to REF are 8–30 % and 18–26 % during day and night, respectively. This is consistent with the larger surface precipitation reduction in region C ($\Delta R = -0.384\,\text{mm day}^{-1}$) compared to region P ($\Delta R = -0.022\,\text{mm day}^{-1}$). Over region C, the significant precipitation reduction could also lead to reduced evaporative cooling below clouds which, in addition to the large increase in cloud-top entrainment rate, contributes to a less humid ($\Delta q_v = -0.2\,\text{g kg}^{-1}$) and warmer ($\Delta T = 0.2\,\text{K}$) MBL.

The larger precipitation inhibition for ScaledEmis over region C is partially related to the prolonged aerosol lifetime due to an increase in in-cloud wet-scavenging timescale (τ). The wet-scavenging timescale for N_{acc} in the MBL is calculated is calculated using:

$$\tau = \frac{\sum\limits_{i,j,k,n} \Delta x \Delta y \Delta z_{i,j,k,n} (Ni_{i,j,k,n} + Nc_{i,j,k,n})}{\sum\limits_{i,j,k,n} \Delta x \Delta y \Delta z_{i,j,k,n} \lambda_{i,j,k,n} Nc_{i,j,k,n}}, \tag{1}$$

where $\mathrm{Ni}_{i,j,k,n}$ and $\mathrm{Nc}_{i,j,k,n}$ are number concentrations of interstitial and cloud-borne accumulation mode particles, respectively; $\lambda_{i,j,k,n}$ is the first-order removal rate for cloud water (s^{-1}), which is equal to the first-order removal rate for cloud-borne aerosol in the model. The Δx and Δy are horizontal grid spacings; Δz is the vertical grid spacing; i and j are horizontal grid indexes; k is the vertical layer index within MBL; and n is the index for hourly outputs. Note that this neglects below-cloud wet-scavenging, but it is negligible for accumulation-mode number. Over region C, with the increased anthropogenic emissions (ScaledEmis), the wet scavenging timescale increases from 2.1 to 4.8 days, more than doubling that of the REF simulation over region C. Wet scavenging is the dominant removal process of aerosols over the clean region, so wet scavenging time scale is a good approximation to aerosol lifetime over this region. The prolonged

ACPD
12, 14623–14667, 2012

aerosol lifetime due to slower wet scavenging is a positive feedback within the system (i.e., more emissions → more CCN → less precipitation → even more CCN).

The day and night differences in POP are small (POP_{night}-POP_{day} < 2 %) over region P, and they are much larger over region C (POP_{night}-POP_{day} = 10–20 % for LWP > 100 g m^{-2}). This larger day-night difference over region C corresponds to the larger amplitude of the surface precipitation diurnal cycle there ($R_{max} - R_{min}$ = 0.836 mm day^{-1}, with R_{max} = 1.06 mm day^{-1} at 5:00 LST and R_{min} = 0.134 day^{-1} at 14:00 LST). The larger day-night differences in precipitation amount and precipitation frequency could be due to the stronger nocturnal convection driven by cloud-top cooling over region C compared to region P.

Cloud effective radius, $r_{e,}$ has been used to characterize the precipitation capacity of clouds. Previous studies (e.g., Freud and Rosenfeld, 2012; Pinsky and Khain, 2002; Rosenfeld et al., 2002) concluded that an r_e value of 14–15 µm is necessary to produce precipitation that is detectable by radar. As shown in the middle columns of Fig. 4, region C has a broader distribution of r_e, and over both regions the POP increases sharply with the increase in r_e once a threshold r_e (∼ 12 µm in REF) is reached. With the same r_e value, POP is larger during the night than during the day, although the day and night POP-r_e relationships resemble each other. Over both regions, anthropogenic aerosols change the POP-r_e relationships, and a more rapid increase in POP with r_e is seen in the 5ANT case compared to the 0ANT case. The threshold r_e, above which the POP starts to increase rapidly with r_e, is also smaller in 5ANT. This indicates the significance of the enhanced anthropogenic emissions in modifying rain processes through changing droplet size spectra.

In stratocumulus clouds, cloud thickness and precipitation are tightly related (e.g., Wang and Feingold, 2009a; Wood, 2007). Region C has more frequent occurrence of thick clouds (D > 400 m), and POP over both regions P and C has a distinct, sharp increasing tendency with increasing cloud thickness for thick clouds. Similar to LWP, clouds with the same thickness have larger POP at night than during the day. Associated with stronger convective mixing driven by cloud-top radiative cooling, the day

ACPD
12, 14623–14667, 2012

and night differences are more distinct over region C (∼ 16 % for $D < 500$ m) than over region P (1–11 % for $D < 500$ m).

Simulated precipitation amounts tend to vary with the selection of cloud microphysics schemes (Boutle and Abel, 2012; Saide et al., 2012). Validation of the simulated precipitation is complicated by spatial variability and uncertainties associated with measurements and derivation approaches. The longitudinal gradient in precipitation is well captured in REF compared to that of observations during VOCALS-REx (Q. Yang et al., 2011). The mean simulated near-surface precipitation rate over the remote region (0.07 mm d^{-1} for 78°–85° W in REF) is in good agreement with the mean radar-derived rain rate at 100 m height (0.06 mm d^{-1} for 80°–85° W; Bretherton et al., 2010). The mean near-surface (∼ 200 m above the ocean surface) rain rates compared well with 2-DC derived rain rates when 75th percentile is used, although they are considerably under-estimated when the mean value is used due to the under-prediction of occasional relatively heavy rain (Bretherton et al., 2010; Q. Yang et al., 2011). We expect that the precipitation frequency response to emissions changes and rain susceptibility over regions P and C are less affected by this possible bias than the simulated precipitation rate.

3.5 Changes in energy fluxes due to anthropogenic and oceanic aerosols

Aerosol and clouds impact the radiative forcing of the atmosphere. At the surface, anthropogenic aerosols have overall cooling effects and sea-salt aerosols have warming effects over the SEP. As shown in Fig. 5, the surface shortwave aerosol forcing (net of direct and indirect effects) is the dominant forcing; it is larger than net changes in surface longwave, latent heat, and sensible heat fluxes due to aerosols. The net shortwave forcing from regional anthropogenic and ocean emissions varies from a net cooling effect near the coast to a net warming effect over the remote ocean. Over region P, where the direct and first indirect effect of aerosols dominate, the changes in surface shortwave fluxes due to regional anthropogenic aerosols is −20 W m^{-2} (15 % of mean aerosol and cloud SF {ACSF} in REF; 5 % albedo increase), and 45 % of this forcing is counteracted by the warming effect of the regional oceanic emissions. For the net shortwave forcing of $-11.2\,\mathrm{W\,m^{-2}}$ from regional emissions (AnthroEmis+OceanEmis), approximately $-4.8\,\mathrm{W\,m^{-2}}$ is from the direct effect that is estimated from their relative contribution to AOD at 550 nm and the offline calculated direct aerosol forcing in REF. This leaves $-6.4\,\mathrm{W\,m^{-2}}$ of indirect effect at the surface over this region although this value is likely to include some non-linear emission responses. The shortwave forcing from regional anthropogenic emissions over region I is much smaller in magnitude ($\sim -3.9\,\mathrm{W\,m^{-2}}$), which is outweighed by the warming effect of the regional oceanic emissions ($6.0\,\mathrm{W\,m^{-2}}$). Over region C, the AnthroEmis and OceanEmis have a net surface warming of $5.0\,\mathrm{W\,m^{-2}}$ from shortwave. This is mainly due to the warming effect of the OceanEmis contribution ($4.0\,\mathrm{W\,m^{-2}}$). The direct aerosol forcing at the surface is approximately $-3.9\,\mathrm{W\,m^{-2}}$ over region C, which indicates a strong warming indirect effect of $\sim 7.9\,\mathrm{W\,m^{-2}}$. The large positive indirect effect is also likely to be associated with meteorological feedback.

The increased anthropogenic emissions (ScaledEmis) exert significant surface cooling with net (direct + indirect) shortwave forcings (SF) of −26 (19 % of ACSF in REF; 6.5 % albedo increase), −25 (18 % of ACSF; 6.0 % albedo increase), and $-45\,\mathrm{W\,m^{-2}}$ (33 % of ACSF; 9.7 % albedo increase) for regions P, I, and C, respectively. This is due to the large changes in cloud optical properties (r_e and COD), macro-physical properties (Z_t, Z_b, D_{cld}, LWP, and f_{low}), and precipitation with the enhanced anthropogenic emissions. The surface shortwave forcing from OceanEmis over the polluted region (region P) is more than double that of the clean region (region C). This is associated with stronger droplet activation suppression by sea-salt particles in the polluted environment, leading to optically thinner clouds (see COD in Fig. 2f).

Figure 6 shows mean net (including direct and indirect effects) shortwave aerosol forcings at the surface versus relative change in N_d due to emission changes for the 9 regions shown in Fig. 1. The mean net (including direct and indirect effects) surface shortwave aerosol forcing over region P is approximately a linear function of the relative change in N_d due to regional anthropogenic emissions (AnthroEmis;

a correlation coefficient {corr} of −0.98). With the enhanced anthropogenic regional emissions (ScaledEmis), regions closer to the coast (regions 1–4; regions 3 and 4 are regions P and I) have shortwave forcing responses that line up around the best-fit line for the AnthroEmis, indicating similar sensitivity. However, over remote regions 5–9 (note that region 6 is region C), the shortwave forcing responses decrease more sharply with the relative change in N_d, with the best-fit line (based on regions 5–9, corr = −0.90) having a much steeper slope (Fig. 6), indicating larger sensitivity of shortwave forcing to anthropogenic aerosols as a result of stronger aerosol-cloud interactions. The mean shortwave response to the oceanic emissions in each region is opposite in sign to that of anthropogenic aerosols. The response is also roughly linear (corr = −0.82) to the relative changes in cloud droplet number concentrations. Due to the different shortwave responses to different (oceanic vs. anthropogenic) emissions and to anthropogenic emissions over clean versus polluted environment, the net aerosol (direct + indirect) shortwave forcing depends on the aerosol-cloud-interaction regimes, the relative abundance of oceanic and anthropogenic aerosols in the mean unperturbed/reference state, and the addition/removal of aerosols through changes in emissions.

The downward surface longwave radiation flux is not sensitive to AnthroEmis. With ScaledEmis, the longwave flux varies from negative ($-1.2\,\mathrm{W\,m^{-2}}$) over region P to positive (1.1 and $3.3\,\mathrm{W\,m^{-2}}$) over regions I and C, corresponding to the changes in f_{low} shown in Fig. 3e. The changes in longwave due to OceanEmis are small and always counteract the changes due to increased regional anthropogenic emissions, which is also similar to the responses of f_{low} in Fig. 3e.

The changes in surface latent heat (Fig. 5c) and sensible heat fluxes (Fig. 5d) due to regional anthropogenic and oceanic aerosols are small ($<5\,\%$ and $<0.5\,\mathrm{W\,m^{-2}}$ in magnitude). With the ScaledEmis, surface fluxes over region C have noticeable response: $-24\,\%$ ($-3.8\,\mathrm{W\,m^{-2}}$) for sensible heat and $2\,\%$ ($3.1\,\mathrm{W\,m^{-2}}$) for latent heat. The small decrease in sensible heat flux and increase in latent heat flux with ScaledEmis

ACPD
12, 14623–14667, 2012

over region C are due to a warmer (by 0.2 K) and drier (of 0.2 g kg^{-1}) MBL and a slight increase (of 0.1 m s^{-1}) in surface wind speed.

4 Summary and conclusion

Changes in aerosol, cloud properties, and energy fluxes over the Southeast Pacific (SEP) due to regional anthropogenic and oceanic emissions are estimated by comparing WRF-Chem simulations under different emission scenarios. Simulations are conducted at a cloud-system resolving scale for the month-long VOCALS-REx period (15 October–16 November 2008). Conclusions and implications from this study are based on the period-averaged responses of aerosols, clouds, and radiation to emission changes relative to the estimated October–November 2008 emissions. Three regions (~ 5° longitude by 5° latitude) with relatively polluted (region P), intermediate (region I), and clean (region C) conditions are selected for detailed analysis. Region I has intermediate anthropogenic impacts, and its response is typically between those of regions P and C, thus the discussion below focuses on regions P and C only.

The near-coast region P is relatively polluted with number concentrations of accumulation mode aerosols near surface (N_a) and cloud droplets at cloud-top (N_d) of 384 and 133 cm^{-3}, resepctively. Regional (within model domain) anthropogenic and oceanic emissions lead to comparable (34 % vs. 20 %) increases in CCN (at 0.1 % supersaturation) number concentrations (N_{CCN}) at 970 hPa over this region. This region is also characterized by stronger suppression of non-sea-salt particle activation by sea-salt particles, the more important role of first than second aerosol indirect effects, low surface precipitation rates (mean of 0.07 mm day^{-1}), and limited impact of aerosols associated with anthropogenic emissions on clouds. Over this region, simulated aerosol size distributions also indicate that the addition of sea-salt particles inhibits the growth of fine non-sea-salt particles (dry diameter < 0.078 µm) to accumulation mode size.

The remote region C is relatively clean (N_a = 221 cm^{-3}; N_d = 71 cm^{-3}) and regional anthropogenic emissions have a negligible impact over this region. This region is also

ACPD

12, 14623–14667, 2012

characterized by large contributions of N_{acc} and N_d from non-local sources (i.e., from the lateral boundaries of the model domain), significant surface precipitation (mean of 0.6 mm day^{-1}), and strong aerosol-cloud-precipitation-radiation interactions when perturbed with a five-fold increase in anthropogenic emissions. The changes in N_{acc} and N_d are not linear functions of the changes in emissions due to the highly non-linear aerosol and cloud microphysical processes.

The effects of regional oceanic emissions on cloud properties, precipitation, and the surface and top-of-atmosphere shortwave fluxes counteract those of anthropogenic aerosols (see Table 2 for a summary of changes in cloud properties). In the polluted region P, a 33 % increase in N_{acc} due to regional anthropogenic emissions leads to a moderate increase in net (direct + indirect) surface aerosol shortwave forcing (15 % of the mean aerosol and cloud SF in REF; 4 % increase in albedo), and 45 % of this effect is counteracted by the warming effect due to oceanic emissions. Due to the varying cloud responses to different emissions (oceanic vs. anthropogenic) and in different regions (clean versus polluted), the net (direct + indirect) shortwave aerosol forcing depends on the aerosol-cloud-interaction regimes, the relative abundance of oceanic and anthropogenic aerosols in the mean unperturbed/reference state, and the addition/removal of aerosols through changes in emissions.

In the clean region, cloud properties have high sensitivity to a moderate increase in aerosol concentrations (ΔN_{acc} = 46 cm^{-3}, {21 %}; ΔN_{CCN} = 13 cm^{-3}, {25 %}) produced by the five-fold increase in regional anthropogenic emissions. Partially associated with the more efficient aerosol activation in a clean environment, the response in cloud micro- and optical properties is large (see Table 2 for a summary). The effect of rain suppression by the enhanced emissions is significant over the remote region C. The reduction in precipitation also prolongs aerosol lifetime in the MBL (4.8 versus 2.1 days), which, in turn, further reduces precipitation. Therefore, the aerosol impact on precipitation is amplified by the positive feedback of precipitation on aerosols. The positive feedback leads to increased sensitivity of clouds and precipitation to emission changes, and thus a stronger ACI regime. The high sensitivity over this region is

ACPD
12, 14623–14667, 2012

also related to a higher entrainment rate increase (16 % over region C versus 3 % at night over region P) due to increased anthropogenic aerosols. Over the clean region, the enhanced anthropogenic emissions lead to an increase in LWP due to the reduced precipitation (as a cloud water sink) and increased surface moisture flux that outweighs the decrease in LWP due to the increased entrainment of dry air.

With the enhanced anthropogenic emissions, aerosol-cloud-precipitation interactions over the clean region C have a strong diurnal cycle with the strongest interactions at night. Based on the simulated mean diurnal cycles, strong solar heating during the day leads to more frequent decoupling of the cloud and sub-cloud layers (diurnal maximum of ∼ 50 %), reduced precipitation (daily minimum of 0.1 mm day^{-1}), thin clouds (daily minimum LWP of ∼ 42 g m^{-2}) near 12:00–15:00 local standard time, and reduced sensitivity of cloud properties to emissions during the daytime. Increased anthropogenic emissions are shown to enhance the daytime decoupling frequency by 5–10 %. The reduced cloud and precipitation sensitivity to emissions during the day over the clean region is also linked to a diurnal N_d minimum (∼ 35 % lower than the diurnal mean).

The high sensitivity to increased anthropogenic emissions over the clean region suggests that the perturbation of the energy balance perturbations from increased anthropogenic emissions are larger in the more susceptible clean environment than in already polluted environment and is larger than possible from first indirect effect alone.

In contrast to short-period and limited-domain process-modeling studies, our month-long regional cloud-system resolving simulation results include the response of clouds and aerosol to varying synoptic conditions. Hence, this series of simulations could provide insights into the aerosol-cloud-precipitation interactions in the context of realistic meteorological conditions, and their impact on climate. We highlight the impacts of anthropogenic emissions on the regional forcing in realistic meteorological conditions, which helps increase the understanding of aerosol effects on climate over the SEP where there are large longitudinal aerosol gradients and the emission sources are rich in sulfur. Our approach of using emission-to-forcing measures and using both relative

ACPD
12, 14623–14667, 2012

and absolute response also facilitates communication between the science community and decision makers.

Acknowledgement. We would like to thank Julia Flaherty for the internal review and Songyou Hong for helpful discussions regarding YSU scheme. Funding for this research has been provided by the US National Oceanic and Atmospheric Administration (NOAA) Atmospheric Composition and Climate Program (NA10AANRG0083/56091). Pacific Northwest National Laboratory is operated by Battelle Memorial Institute for the US Department of Energy under Contract No. DE-AC05-76RL01830.

References

Ackerman, A. S., Toon, O. B., Stevens, D. E., and Coakley, J. A.: Enhancement of cloud cover and suppression of nocturnal drizzle in stratocumulus polluted by haze, Geophys. Res. Lett., 30, 1381, doi:10.1029/2002gl016634, 2003.

Ackerman, A. S., Kirkpatrick, M. P., Stevens, D. E., and Toon, O. B.: The impact of humidity above stratiform clouds on indirect aerosol climate forcing, Nature, 432, 1014–1017, doi:10.1038/Nature03174, 2004.

Albrecht, B. A.: Aerosols, cloud microphysics, and fractional cloudiness, Science, 245, 1227–1230, 1989.

Allen, G., Coe, H., Clarke, A., Bretherton, C., Wood, R., Abel, S. J., Barrett, P., Brown, P., George, R., Freitag, S., McNaughton, C., Howell, S., Shank, L., Kapustin, V., Brekhovskikh, V., Kleinman, L., Lee, Y.-N., Springston, S., Toniazzo, T., Krejci, R., Fochesatto, J., Shaw, G., Krecl, P., Brooks, B., McMeeking, G., Bower, K. N., Williams, P. I., Crosier, J., Crawford, I., Connolly, P., Allan, J. D., Covert, D., Bandy, A. R., Russell, L. M., Trembath, J., Bart, M., McQuaid, J. B., Wang, J., and Chand, D.: South East Pacific atmospheric composition and variability sampled along 20° S during VOCALS-REx, Atmos. Chem. Phys., 11, 5237–5262, doi:10.5194/acp-11-5237-2011, 2011.

Baker, M. B. and Charlson, R. J.: Bistability of CCN concentrations and thermodynamics in the cloud-topped boundary-layer, Nature, 345, 142–145, 1990.

Barnard, J. C., Fast, J. D., Paredes-Miranda, G., Arnott, W. P., and Laskin, A.: Technical Note: Evaluation of the WRF-Chem "Aerosol Chemical to Aerosol Optical Properties" Module using

ACPD

12, 14623–14667, 2012

Aerosol impact on clouds and precipitation

Q. Yang et al.

data from the MILAGRO campaign, Atmos. Chem. Phys., 10, 7325–7340, doi:10.5194/acp-10-7325-2010, 2010.
Berner, A. H., Bretherton, C. S., and Wood, R.: Large-eddy simulation of mesoscale dynamics and entrainment around a pocket of open cells observed in VOCALS-REx RF06, Atmos. Chem. Phys., 11, 10525–10540, doi:10.5194/acp-11-10525-2011, 2011.
Blomquist, B. W., Fairall, C. W., Huebert, B. J., Kieber, D. J., and Westby, G. R.: DMS sea-air transfer velocity: direct measurements by eddy covariance and parameterization based on the NOAA/COARE gas transfer model, Geophys. Res. Lett., 33, L07601, doi:10.1029/2006gl025735, 2006.
Bretherton, C. S. and Wyant, M. C.: Moisture transport, lower-tropospheric stability, and decoupling of cloud-topped boundary layers, J. Atmos. Sci., 54, 148–167, 1997.
Bretherton, C. S., Blossey, P. N., and Uchida, J.: Cloud droplet sedimentation, entrainment efficiency, and subtropical stratocumulus albedo, Geophys. Res. Lett., 34, L03813, doi:10.1029/2006gl027648, 2007.
Bretherton, C. S., Wood, R., George, R. C., Leon, D., Allen, G., and Zheng, X.: Southeast Pacific stratocumulus clouds, precipitation and boundary layer structure sampled along 20° S during VOCALS-REx, Atmos. Chem. Phys., 10, 10639–10654, doi:10.5194/acp-10-10639-2010, 2010.
Chand, D., Hegg, D. A., Wood, R., Shaw, G. E., Wallace, D., and Covert, D. S.: Source atrribution of climatically important aerosol properties measured at Paposo (Chile) during VOCALS, Atmos. Chem. Phys., 10, 10789–19091, doi:10.5194/acp-10-10789-2010, 2010.
Chapman, E. G., Gustafson Jr., W. I., Easter, R. C., Barnard, J. C., Ghan, S. J., Pekour, M. S., and Fast, J. D.: Coupling aerosol-cloud-radiative processes in the WRF-Chem model: investigating the radiative impact of elevated point sources, Atmos. Chem. Phys., 9, 945–964, doi:10.5194/acp-9-945-2009, 2009.
Charlson, R. J., Lovelock, J. E., Andreae, M. O., and Warren, S. G.: Oceanic phytoplankton, atmospheric sulfur, cloud albedo and climate, Nature, 326, 655–661, 1987.
Chen, Y.-C., Xue, L., Lebo, Z. J., Wang, H., Rasmussen, R. M., and Seinfeld, J. H.: A comprehensive numerical study of aerosol-cloud-precipitation interactions in marine stratocumulus, Atmos. Chem. Phys., 11, 9749–9769, doi:10.5194/acp-11-9749-2011, 2011.
Clarke, A. D., Owens, S. R., and Zhou, J. C.: An ultrafine seasalt flux from breaking waves: implications for cloud condensa- tion nuclei in the remote marine atmosphere, J. Geophys. Res.-Atmos., 111, D06202, doi:10.1029/2005jd006565, 2006.

ACPD
12, 14623–14667, 2012

Fast, J. D., Gustafson, W. I., Easter, R. C., Zaveri, R. A., Barnard, J. C., Chapman, E. G., Grell, G. A., and Peckham, S. E.: Evolution of ozone, particulates, and aerosol direct radiative forcing in the vicinity of Houston using a fully coupled meteorology-chemistry-aerosol model, J. Geophys. Res.-Atmos., 111, D21305, doi:10.1029/2005jd006721, 2006.

Fast, J. D., Gustafson, W. I., Berg, L. K., Shaw, W. J., Pekour, M., Shrivastava, M., Barnard, J. C., Ferrare, R. A., Hostetler, C. A., Hair, J. A., Erickson, M., Jobson, B. T., Flowers, B., Dubey, M. K., Springston, S., Pierce, R. B., Dolislager, L., Pederson, J., and Zaveri, R. A.: Transport and mixing patterns over Central California during the carbonaceous aerosol and radiative effects study (CARES), Atmos. Chem. Phys., 12, 1759–1783, doi:10.5194/acp-12-1759-2012, 2012.

Feingold, G., Cotton, W. R., Kreidenweis, S. M., and Davis, J. T.: The impact of giant cloud condensation nuclei on drizzle formation in stratocumulus: implications for cloud radiative properties, J. Atmos. Sci., 56, 4100–4117, 1999.

Feingold, G., Remer, L. A., Ramaprasad, J., and Kaufman, Y. J.: Analysis of smoke impact on clouds in Brazilian biomass burning regions: an extension of Twomey's approach, J. Geophys. Res., 106, 22907–22922, 2001.

Feingold, G., Eberhard, W. L., Veron, D. E., and Previdi, M.: First measurements of the Twomey indirect effect using ground-based remote senors, Geophys. Res. Lett., 30, 1287, doi:10.1029/2002GL016633, 2003.

Freud, E. and Rosenfeld, D.: Linear relation between convective cloud drop number concentration and depth for rain initiation, J. Geophys. Res.-Atmos., 117, D02207, doi:10.1029/2011jd016457, 2012.

Gao, Y., Liu, X., Zhao, C., and Zhang, M.: Emission controls versus meteorological conditions in determining aerosol concentrations in Beijing during the 2008 Olympic Games, Atmos. Chem. Phys., 11, 12437–12451, doi:10.5194/acp-11-12437-2011, 2011.

Ghan, S. J., Guzman, G., and Abdul-Razzak, H.: Competition between sea salt and sulfate particles as cloud condensation nuclei, J. Atmos. Sci., 55, 3340–3347, 1998.

Gong, S. L., Barrie, L. A., and Blanchet, J. P.: Modeling sea-salt aerosols in the atmosphere. 1. Model development, J. Geophys. Res.-Atmos., 102, 3805–3818, 1997.

Grell, G. A., Peckham, S. E., Schmitz, R., McKeen, S. A., Frost, G., Skamarock, W. C., and Eder, B.: Fully coupled "online" chemistry within the WRF model, Atmos. Environ., 39, 6957–6975, doi:10.1016/j.atmosenv.2005.04.027, 2005.

ACPD
12, 14623–14667, 2012

Aerosol impact on clouds and precipitation

Q. Yang et al.

Gustafson, W. I., Chapman, E. G., Ghan, S. J., Easter, R. C., and Fast, J. D.: Impact on modeled cloud characteristics due to simplified treatment of uniform cloud condensation nuclei during NEAQS 2004, Geophys. Res. Lett., 34, L19809, doi:10.1029/2007gl030021, 2007.

Hawkins, L. N., Russell, L. M., Covert, D. S., Quinn, P. K., and Bates, T. S.: Carboxylic acids, sulfates, and organosulfates in processed continental organic aerosol over the southeast Pacific Ocean during VOCALS-REx 2008, J. Geophys. Res.-Atmos., 115, D13201, doi:10.1029/2009jd013276, 2010.

Hill, A. A., Feingold, G., and Jiang, H. L.: The influence of entrainment and mixing assumption on aerosol-cloud interactions in marine stratocumulus, J. Atmos. Sci., 66, 1450–1464, doi:10.1175/2008jas2909.1, 2009.

Hong, S. Y., Noh, Y., and Dudhia, J.: A new vertical diffusion package with an explicit treatment of entrainment processes, Mon. Weather Rev., 134, 2318–2341, 2006.

Jones, C. R., Bretherton, C. S., and Leon, D.: Coupled vs. decoupled boundary layers in VOCALS-REx, Atmos. Chem. Phys., 11, 7143–7153, doi:10.5194/acp-11-7143-2011, 2011.

Kazil, J., Wang, H., Feingold, G., Clarke, A. D., Snider, J. R., and Bandy, A. R.: Modeling chemical and aerosol processes in the transition from closed to open cells during VOCALS-REx, Atmos. Chem. Phys., 11, 7491–7514, doi:10.5194/acp-11-7491-2011, 2011.

Klein, S. A. and Hartmann, D. L.: The seasonal cycle of low stratiform clouds, J. Climate, 6, 1587–1606, 1993.

Kleinman, L. I., Daum, P. H., Lee, Y.-N., Lewis, E. R., Sedlacek III, A. J., Senum, G. I., Springston, S. R., Wang, J., Hubbe, J., Jayne, J., Min, Q., Yum, S. S., and Allen, G.: Aerosol concentration and size distribution measured below, in, and above cloud from the DOE G-1 during VOCALS-REx, Atmos. Chem. Phys., 12, 207–223, doi:10.5194/acp-12-207-2012, 2012.

L'ecuyer, T. S., Berg, W., Haynes, J., Lebsock, M., and Takemura, T.: Global observations of aerosol impacts on precipitation occurrence in warm maritime clouds, J. Geophys. Res.-Atmos., 114, D09211, doi:10.1029/2008jd011273, 2009.

Lu, M. L. and Seinfeld, J. H.: Study of the aerosol indirect effect by large-eddy simulation of marine stratocumulus, J. Atmos. Sci., 62, 3909–3932, 2005.

Matsui, T., Masunaga, H., Kreidenweis, S. M., Pielke, R. A., Tao, W. K., Chin, M., and Kaufman, Y. J.: Satellite-based assessment of marine low cloud variability associated with aerosol, atmospheric stability, and the diurnal cycle (vol 111, art no D17204, 2006), J. Geophys. Res.-Atmos., 111, D20202, doi:10.1029/2006jd008056, 2006.

Mechem, D. B., Yuter, S. E., and de Szoeke, S. P.: Thermodynamic and aerosol controls in Southeast Pacific Stratocumulus, J. Atmos. Sci., 69, 1250–1266, doi:10.1175/JAS-D-11-0165.1, 2012.

Monahan, E. C., Spiel, D. E., and Davidson, K. L.: A model of marine aerosol generation via whitecaps and wave disruption, in: Oceanic Whitecaps, edited by: Monahan, E. C. and Niocail, G. M., D. Reidel, Norwell, 167–174, 1986.

Morrison, H., Thompson, G., and Tatarskii, V.: Impact of cloud microphysics on the development of trailing stratiform precipitation in a simulated squall line: comparison of one- and two-moment schemes, Mon. Weather Rev., 137, 991–1007, doi:10.1175/2008mwr2556.1, 2009.

Nicholls, S.: The dynamics of stratocumulus – aircraft observations and comparisons with a mixed layer model, Q. J. Roy. Meteorol. Soc., 110, 783–820, 1984.

Nightingale, P. D., Malin, G., Law, C. S., Watson, A. J., Liss, P. S., Liddicoat, M. I., Boutin, J., and Upstill-Goddard, R. C.: In situ evaluation of air-sea gas exchange parameterizations using novel conservative and volatile tracers, Global Biogeochem. Cy., 14, 373–387, 2000.

Noh, Y., Gheon, W. G., Hong, S. Y., and Raasch, S.: Improvement of the K-profile model for the planetary boundary layer based on large eddy simulation data, Bound.-Layer Meteorol., 107, 401–427, 2003.

Painemal, D. and Zuidema, P.: Microphysical variability in southeast Pacific Stratocumulus clouds: synoptic conditions and radiative response, Atmos. Chem. Phys., 10, 6255–6269, doi:10.5194/acp-10-6255-2010, 2010.

Pincus, R. and Baker, M. B.: Effect of precipitation on the albedo susceptibility of clouds in the marine boundary-layer, Nature, 372, 250–252, 1994.

Pinsky, M. B. and Khain, A. P.: Effects of in-cloud nucleation and turbulence on droplet spectrum formation in cumulus clouds, Q. J. Roy. Meteorol. Soc., 128, 501–533, 2002.

Posselt, R. and Lohmann, U.: Influence of Giant CCN on warm rain processes in the ECHAM5 GCM, Atmos. Chem. Phys., 8, 3769–3788, doi:10.5194/acp-8-3769-2008, 2008.

Qian, Y., Gustafson, W. I., Leung, L. R., and Ghan, S. J.: Effects of soot-induced snow albedo change on snowpack and hydrological cycle in Western United States based on Weather Research and Forecasting chemistry and regional climate simulations, J. Geophys. Res.-Atmos., 114, D03108, doi:10.1029/2008jd011039, 2009.

Quaas, J., Ming, Y., Menon, S., Takemura, T., Wang, M., Penner, J. E., Gettelman, A., Lohmann, U., Bellouin, N., Boucher, O., Sayer, A. M., Thomas, G. E., McComiskey, A., Feingold, G., Hoose, C., Kristjánsson, J. E., Liu, X., Balkanski, Y., Donner, L. J., Ginoux, P. A.,

ACPD

12, 14623–14667, 2012

Stier, P., Grandey, B., Feichter, J., Sednev, I., Bauer, S. E., Koch, D., Grainger, R. G., Kirkevåg, A., Iversen, T., Seland, Ø., Easter, R., Ghan, S. J., Rasch, P. J., Morrison, H., Lamarque, J.-F., Iacono, M. J., Kinne, S., and Schulz, M.: Aerosol indirect effects – general circulation model intercomparison and evaluation with satellite data, Atmos. Chem. Phys., 9, 8697–8717, doi:10.5194/acp-9-8697-2009, 2009.

Loeb, N. G. and Schuster, G. L.: An observational study of the relationship between cloud, aerosol and meteorology in broken low-level cloud conditions, J. Geophys. Res., 113, D14214, doi:10.1029/2007JD009763, 2008.

Raes, F.: Entrainment of free tropospheric aerosols as a regulating mechanism for cloud condensation nuclei in the remote marine boundary layer, J. Geophys. Res., 100(D2), 2893–2903, doi:10.1029/94JD02832, 1995.

Rahn, D. A. and Garreaud, R.: Marine boundary layer over the subtropical southeast Pacific during VOCALS-REx – Part 1: Mean structure and diurnal cycle, Atmos. Chem. Phys., 10, 4491–4506, doi:10.5194/acp-10-4491-2010, 2010.

Rosenfeld, D., Lahav, R., Khain, A., and Pinsky, M.: The role of sea spray in cleansing air pollution over ocean via cloud processes, Science, 297, 1667–1670, doi:10.1126/Science.1073869, 2002.

Sandu, I., Brenguier, J. L., Geoffroy, O., Thouron, O., and Masson, V.: Aerosol impacts on the diurnal cycle of marine stratocumulus, J. Atmos. Sci., 65, 2705–2718, doi:10.1175/2008jas2451.1, 2008.

Shank, L. M., Howell, S., Clarke, A. D., Freitag, S., Brekhovskikh, V., Kapustin, V., McNaughton, C., Campos, T., and Wood, R.: Organic matter and non-refractory aerosol over the remote Southeast Pacific: oceanic and combustion sources, Atmos. Chem. Phys., 12, 557–576, doi:10.5194/acp-12-557-2012, 2012.

Shin, H. H. and Hong, S.-Y.: Intercomparison of planetary boundary-layer parameterization in the WRF Model for a single day from CASE-99, Bound.-Layer Meteorol., 139, 261–281, doi:10.1007/s10546-010-9583-z, 2011.

Solomon, S., Qin, D., Manning, M., Chen, Z., Marquis, M., Averyt, K., Tignor, M., and Miller, H. L. (eds.): IPCC, 2007: Summary for Policymakers, in: Climate Change 2007: The Physical Science Basis. Contribution of Working Group I to the Fourth Assessment Report of the Intergovernmental Panel on Climate Change, Cambridge University Press, Cambridge, UK and New York, NY, USA, 2007.

Sorooshian, A., Feingold, G., Lebsock, M. D., Jiang, H. L., and Stephens, G. L.: On the precipitation susceptibility of clouds to aerosol perturbations, Geophys. Res. Lett., 36, L13803, doi:10.1029/2009gl038993, 2009.

Stevens, B.: Bulk boundary-layer concepts for simplified models of tropical dynamics, Theor. Comp. Fluid Dyn., 20, 279–304, doi:10.1007/S00162-006-0032-Z, 2006.

Stevens, B. and Feingold, G.: Untangling aerosol effects on clouds and precipitation in a buffered system, Nature, 461, 607–613, doi:10.1038/nature08281, 2009.

de Szoeke, S. P., Fairall, C. W., Wolfe, D. E., Bariteau, L., and Zuidema, P.: Surface flux observations on the Southeastern Tropical Pacific Ocean and attribution of SST errors in coupled ocean-atmosphere models, J. Climate, 23, 4152–4174, doi:10.1175/2010jcli3411.1, 2010.

Terai, C. R., Wood, R., Leon, D. C., and Zuidema, P.: Does precipitation susceptibility vary with increasing cloud thickness in marine stratocumulus?, Atmos. Chem. Phys., 12, 4567–4583, doi:10.5194/acp-12-4567-2012, 2012.

Thomas, M. A., Suntharalingam, P., Pozzoli, L., Devasthale, A., Kloster, S., Rast, S., Feichter, J., and Lenton, T. M.: Rate of non-linearity in DMS aerosol-cloud-climate interactions, Atmos. Chem. Phys., 11, 11175–11183, doi:10.5194/acp-11-11175-2011, 2011.

Twomey, S.: Influence of pollution on shortwave albedo of clouds, J. Atmos. Sci., 34, 1149–1152, 1977.

Wang, H. and Feingold, G.: Modeling mesoscale cellular structures and drizzle in marine stratocumulus. Part I: Impact of drizzle on the formation and evolution of open cells, J. Atmos. Sci., 66, 3237–3256, doi:10.1175/2009jas3022.1, 2009a.

Wang, H. and Feingold, G.: Modeling mesoscale cellular structures and drizzle in marine stratocumulus. Part II: the microphysics and dynamics of the boundary region between open and closed cells, J. Atmos. Sci., 66, 3257–3275, doi:10.1175/2009jas3120.1, 2009b.

Wang, H. and McFarquhar, G. M.: Modeling aerosol effects on shallow cumulus convection under various meteorological conditions observed over the Indian Ocean and implications for development of mass-flux parameterizations for climate models, J. Geophys. Res.-Atmos., 113, D20201, doi:10.1029/2008jd009914, 2008a.

Wang, H. and McFarquhar, G. M.: Large-eddy simulations of the diurnal cycle of shallow convection and cloudiness over the tropical Indian Ocean, Q. J. Roy. Meteorol. Soc., 134, 643–661, doi:10.1002/Qj.238, 2008b.

ACPD
12, 14623–14667, 2012

Wang, M., Ghan, S., Ovchinnikov, M., Liu, X., Easter, R., Kassianov, E., Qian, Y., and Morrison, H.: Aerosol indirect effects in a multi-scale aerosol-climate model PNNL-MMF, Atmos. Chem. Phys., 11, 5431–5455, doi:10.5194/acp-11-5431-2011, 2011.

Wood, R.: Cancellation of aerosol indirect effects in marine stratocumulus through cloud thinning, J. Atmos. Sci., 64, 2657–2669, doi:10.1175/Jas3942.1, 2007.

Wood, R., Bretherton, C. S., Leon, D., Clarke, A. D., Zuidema, P., Allen, G., and Coe, H.: An aircraft case study of the spatial transition from closed to open mesoscale cellular convection over the Southeast Pacific, Atmos. Chem. Phys., 11, 2341–2370, doi:10.5194/acp-11–2341-2011, 2011a.

Wood, R., Mechoso, C. R., Bretherton, C. S., Weller, R. A., Huebert, B., Straneo, F., Albrecht, B. A., Coe, H., Allen, G., Vaughan, G., Daum, P., Fairall, C., Chand, D., Klenner, L. G., Garreaud, R., Grados, C., Covert, D. S., Bates, T. S., Krejci, R., Russell, L. M., de Szoeke, S., Brewer, A., Yuter, S. E., Springston, S. R., Chaigneau, A., Toniazzo, T., Minnis, P., Palikonda, R., Abel, S. J., Brown, W. O. J., Williams, S., Fochesatto, J., Brioude, J., and Bower, K. N.: The VAMOS Ocean-Cloud-Atmosphere-Land Study Regional Experiment (VOCALS-REx): goals, platforms, and field operations, Atmos. Chem. Phys., 11, 627–654, doi:10.5194/acp-11-627-2011, 2011b.

Woodhouse, M. T., Carslaw, K. S., Mann, G. W., Vallina, S. M., Vogt, M., Halloran, P. R., and Boucher, O.: Low sensitivity of cloud condensation nuclei to changes in the sea-air flux of dimethyl-sulphide, Atmos. Chem. Phys., 10, 7545–7559, doi:10.5194/Acp-10-7545-2010, 2010.

Yang, M., Blomquist, B. W., and Huebert, B. J.: Constraining the concentration of the hydroxyl radical in a stratocumulus-topped marine boundary layer from sea-to-air eddy covariance flux measurements of dimethylsulfide, Atmos. Chem. Phys., 9, 9225–9236, doi:10.5194/acp-9-9225-2009, 2009.

Yang, M., Huebert, B. J., Blomquist, B. W., Howell, S. G., Shank, L. M., McNaughton, C. S. D., Clarke, A., Hawkins, L. N., Russell, L. M., Covert, D. S., Coffman, D. J., Bates, T. S., Quinn, P. K., Zagorac, N., Bandy, A. R., de Szoeke, S. P., Zuidema, P. D., Tucker, S. C., Brewer, W. A., Benedict, K. B., and Collett, J. L.: Atmospheric sulfur cycling in the Southeastern Pacific – longitudinal distribution, vertical profiel, and diel variability observed during VOCALS-REx, Atmos. Chem. Phys., 11, 5079–5097, doi:10.5194/acp-11-5079-2011, 2011.

Yang, Q., Gustafson, W. I., Fast, J. D., Wang, H., Easter, R. C., Morrison, H., Lee, Y. N., Chapman, E. G., Spak, S. N., and Mena-Carrasco, M. A.: Assessing regional scale predictions

of aerosols, marine stratocumulus, and their interactions during VOCALS-REx using WRF-Chem, Atmos. Chem. Phys., 11, 11951–11975, doi:10.5194/Acp-11-11951-2011, 2011.
Zaveri, R. A., Easter, R. C., Fast, J. D., and Peters, L. K.: Model for Simulating Aerosol Interactions and Chemistry (MOSAIC), J. Geophys. Res.-Atmos., 113, D13204, doi:10.1029/2007jd008782, 2008.
Zhang, Y., Wen, X. Y., and Jang, C. J.: Simulating chemistry-aerosol-cloud-radiation-climate feedbacks over the continental US using the online-coupled Weather Research Forecasting Model with chemistry (WRF/Chem), Atmos. Environ., 44, 3568–3582, doi:10.1016/J.Atmosenv.2010.05.056, 2010.
Zheng, X., Albrecht, B., Jonsson, H. H., Khelif, D., Feingold, G., Minnis, P., Ayers, K., Chuang, P., Donaher, S., Rossiter, D., Ghate, V., Ruiz-Plancarte, J., and Sun-Mack, S.: Observations of the boundary layer, cloud, and aerosol variability in the southeast Pacific near-coastal marine stratocumulus during VOCALS-REx, Atmos. Chem. Phys., 11, 9943–9959, doi:10.5194/acp-11-9943-2011, 2011.
Zuidema, P., Leon, D., Pazmany, A., and Cadeddu, M.: Aircraft millimeter-wave passive sensing of cloud liquid water and water vapor during VOCALS-REx, Atmos. Chem. Phys. 12, 355–369, doi:10.5194/acp-12-355-2012, 2012.

ACPD
12, 14623–14667, 2012

Aerosol impact on clouds and precipitation

Q. Yang et al.

ACPD
12, 14623–14667, 2012

Table 1. Description of four primary model simulations.

Simulations	Emissions included	Description of simulations
REF	AnthroEmis +OceanEmis	Standard/reference simulation
0OCE	AnthroEmis	Sea salt and DMS emissions turned off
0ANT	OceanEmis	Anthropogenic emissions turned off
5ANT	ScaledEmis	Anthropogenic emissions scaled by a factor of 5

Table 2. The mean responses and aerosol-cloud interaction indices associated with regional oceanic (OceanEmis), regional anthropogenic (AnthroEmis), and enhanced regional anthropogenic emissions (ScaledEmis).

Parameter	Region	OceanEmis		AnthroEmis		ScaledEmis	
		Response	$ACI_{CCN}(Y)$	Response	$ACI_{CCN}(Y)$	Response	$ACI_{CCN}(Y)$
ΔN_d	P	−27 %	−1.09	34 %	1.00	72 %	0.83
	C	−3 %	−0.09	0 %	–	36 %	1.36
Δr_e	P	5 %	0.24	−10 %	−0.25	−21 %	−0.37
	C	1 %	0.03	–	–	−32 %	−1.71
ΔCOD	P	−9 %	−0.42	14 %	0.36	21 %	0.29
	C	−4 %	−0.07	–	–	54 %	1.90
ΔZ_t	P	−1 %	−0.06	1 %	0.03	6 %	0.10
	C	−1 %	−0.02	–	–	13 %	0.56
ΔD_{cld}	P	0 %	−0.02	0 %	0.01	0 %	0.00
	C	0 %	−0.01	–	–	11 %	0.48
ΔLWP	P	−1 %	−0.05	2 %	0.06	2 %	0.03
	C	−2 %	−0.04	–	–	41 %	1.52

ACPD
12, 14623–14667, 2012

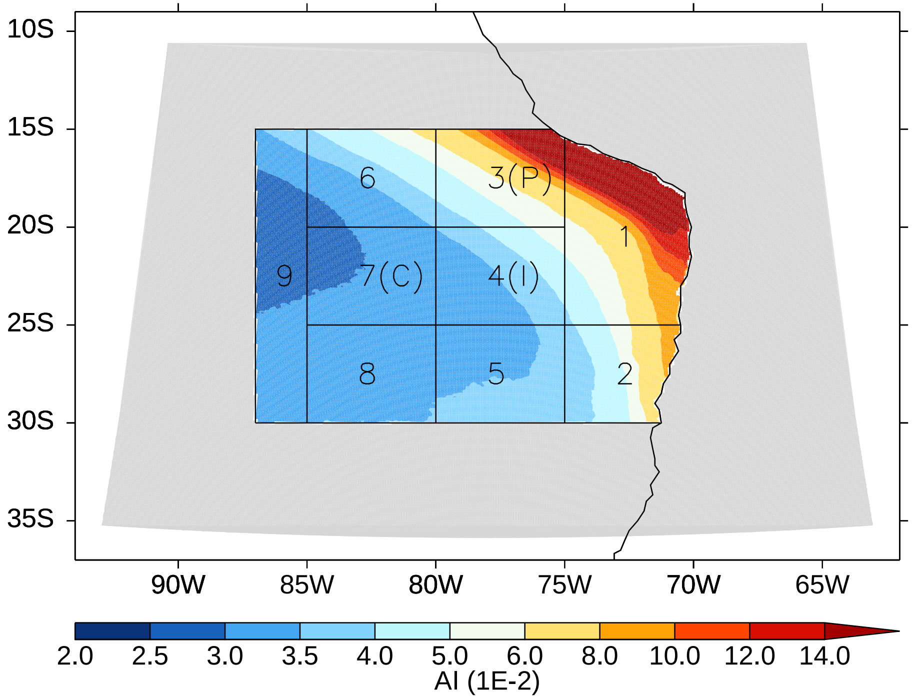

Fig. 1. Monthly average aerosol indexes (AI) during the VOCALS-REx period. The modeling domain is divided into 9 regions (numbered by 1–9) with the regions 3–8 being 5° × 5° in sizes. Regions 3, 4, and 7 are also referred as polluted (P), intermediate (I), and clean (C) regions in the main text. The grey area shows the model domain. Areas too close to the lateral boundaries are not included in this study.

ACPD
12, 14623–14667, 2012

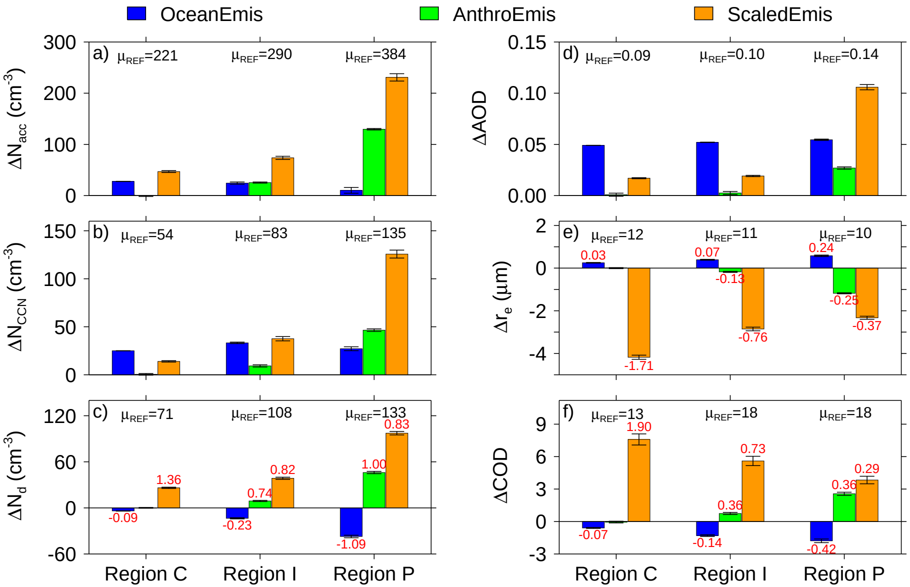

Fig. 2. Changes in mean accumulation mode aerosol (N_a, **a**), CCN (N_{ccn} at 0.1 % supersaturation and on 975 hP, **b**), cloud droplet number (N_d, **c**), aerosol optical depth (AOD, **d**), cloud top effective radius (r_e, **e**), and cloud optical depth (COD, **f**) due to ocean emissions (OceanEmis, blue), anthropogenic emissions (AnthroEmis, green), and scaled anthropogenic emissions (ScaledEmis, orange) within the model domain. The mean values in the reference simulation (REF) are shown at the top of each panel for each region (regions P, I, and C). The cloud property changes are also calculated as $\frac{\Delta \ln(Y)}{\Delta \ln(N_{cnn})}$ and the values are shown in red above or below each color bar, where Y is the cloud property. The error bars are provided as the $\pm 2\sigma$ where (σ is the standard deviation of the mean changes).

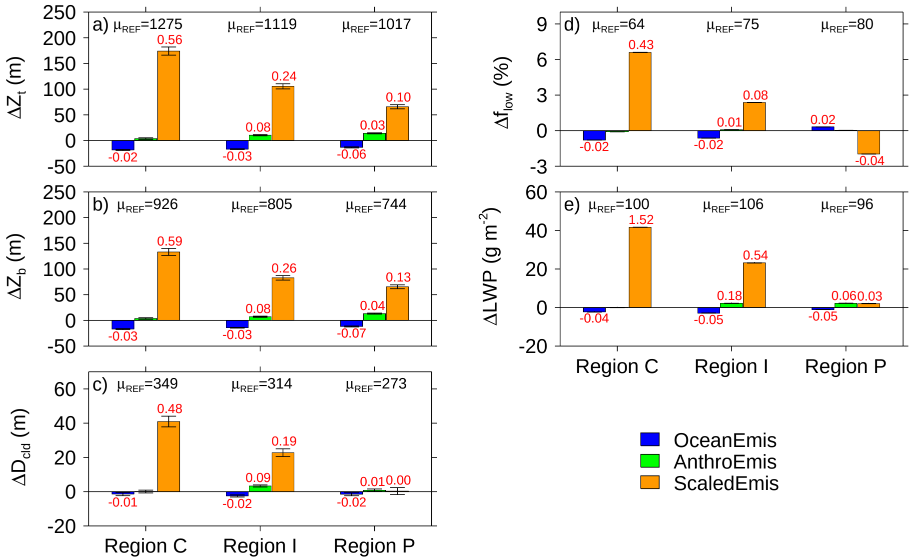

Fig. 3. Changes in mean cloud top height (Z_t, **a**), cloud base height (Z_b, **b**), cloud depth (D_{cld}, **c**), liquid water path (LWP, **d**), and low cloud fraction (f_{low}, **e**) due to ocean emissions (OceanEmis, blue), anthropogenic emissions (AnthroEmis, green), and scaled anthropogenic emissions (ScaledEmis, and orange) within the model domain. The mean values in the reference simulation (REF) are shown at the top of each panel for each region (regions P, I, and C). The cloud property changes are also calculated as $\frac{\Delta \ln(Y)}{\Delta \ln(N_{cnn})}$ and the values are shown in red above or below each color bar, where Y is the cloud property.

ACPD
12, 14623–14667, 2012

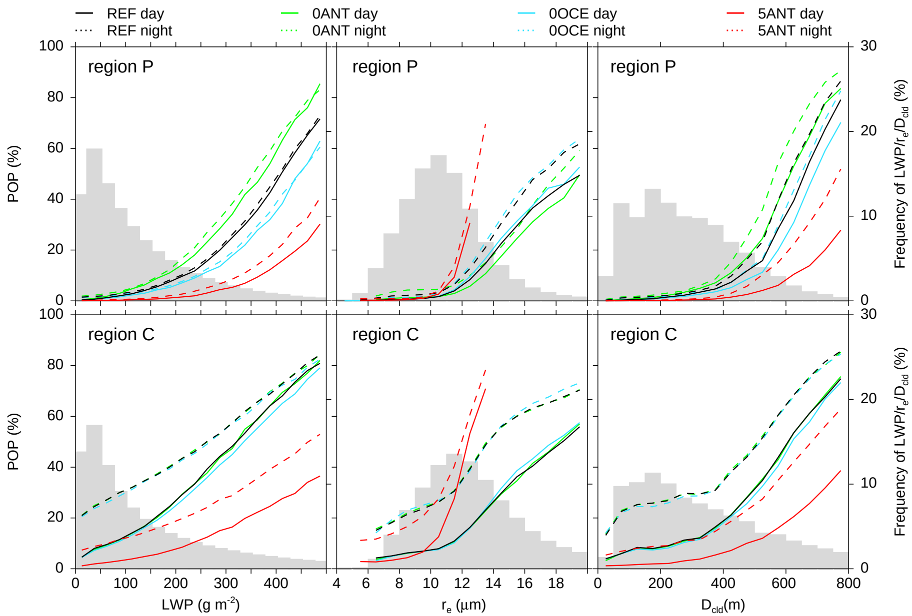

Fig. 4. Relationships between the probability of precipitation (POP) and liquid water path (LWP, left), cloud top effective radius (r_e, middle) and cloud thickness (D, right) during the day (solid lines) and the night (dashed lines) in the reference simulation (REF, black) and in the 3 sensitivity simulations with regional anthropogenic emissions turned off (0ANT, green), with regional oceanic emissions turned off (0OCE, blue), and with scaled regional anthropogenic emissions (5ANT, red), respectively, for two regions with low (region P) and high (region C) aerosol-cloud interactions. The histograms of LWP (left), r_e (middle), and D (right) in the REF simulation are shown as the grey shaded areas. The figure is calculated based on hourly outputs on each model grid.

ACPD
12, 14623–14667, 2012

Aerosol impact on clouds and precipitation

Q. Yang et al.

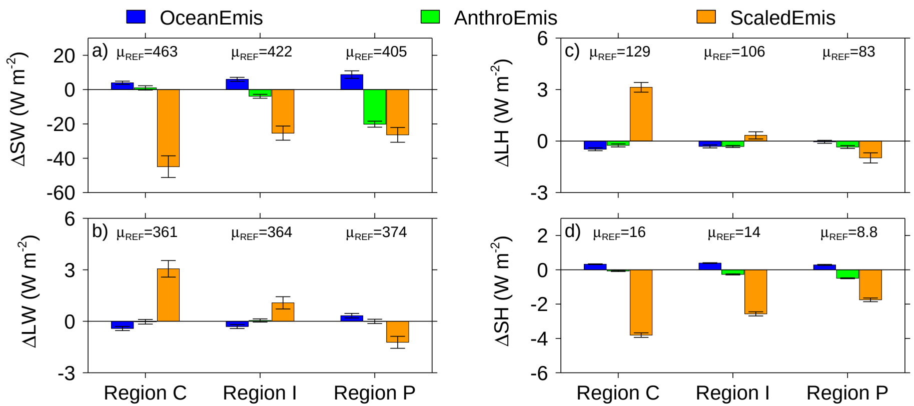

Fig. 5. Changes in mean surface energy fluxes including downward shortwave (SW, **a**), downward longwave (LW, **b**), latent heat (LH, **c**), and sensible heat (SH; panel d) due to ocean emissions (OceanEmis, blue), anthropogenic emissions (AnthroEmis, green), and scaled anthropogenic emissions (ScaledEmis, orange) within the model domain. The mean values in the reference simulation (REF) are shown at the top of each panel for each region (regions P, I, and C). Note the different scales used in y-axis.

ACPD
12, 14623–14667, 2012

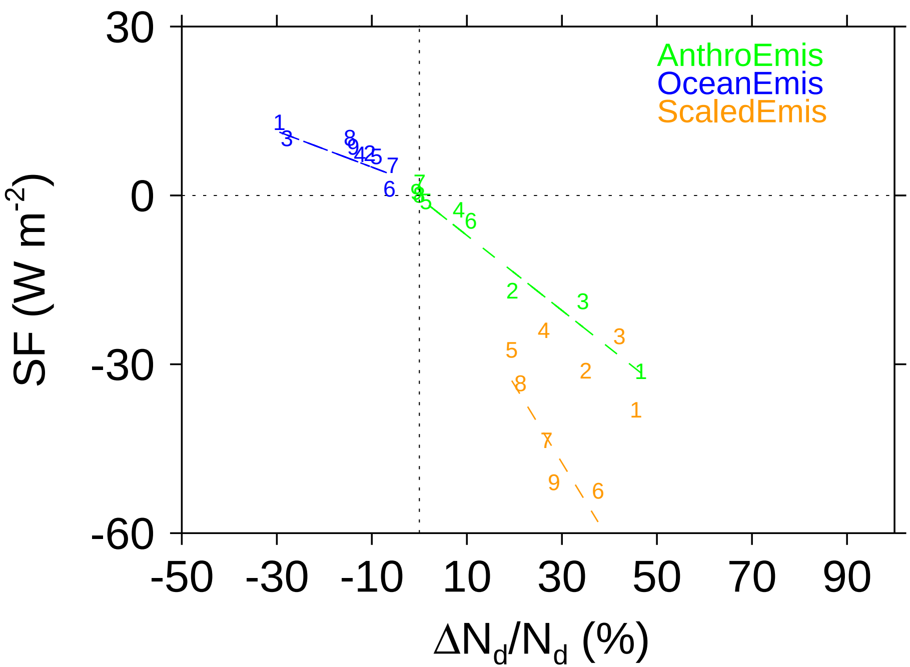

Fig. 6. Relationships between mean relative changes in droplet number concentrations and mean surface shortwave forcings (SF) due to ocean emissions (OceanEmis, blue), anthropogenic emissions (AnthroEmis, green), and scaled anthropogenic emissions (ScaledEmis, orange) within the model domain for the 9 regions defined in Fig. 1. The green and blue best fit lines are based on the green and blue data points, and the orange color line is based on orange data points for regions 5–9 only.

ACPD
12, 14623–14667, 2012